.

Influence of Excitation Pulse Duration on the Efficiency of Upconversion Nanoparticle-Based FRET

Electronic Supplementary Information (ESI)

Alejandro Casillas-Rubio,[a] Khouloud Hamraoui,[b] Diego Mendez-Gonzalez,[b] Marco Laurenti,[b] Jorge Rubio-Retama,[b] Oscar G. Calderón,*[a] and Sonia Melle,*[a]

Contents

[a] *Department of Optics, Complutense University of Madrid, E-28037 Madrid, Spain*
[b] *Department of Chemistry in Pharmaceutical Sciences, Complutense University of Madrid, E-28040 Madrid, Spain*

S1. Z-Potential of UCNPs-PAA and UCNPs-PAA-PEI.

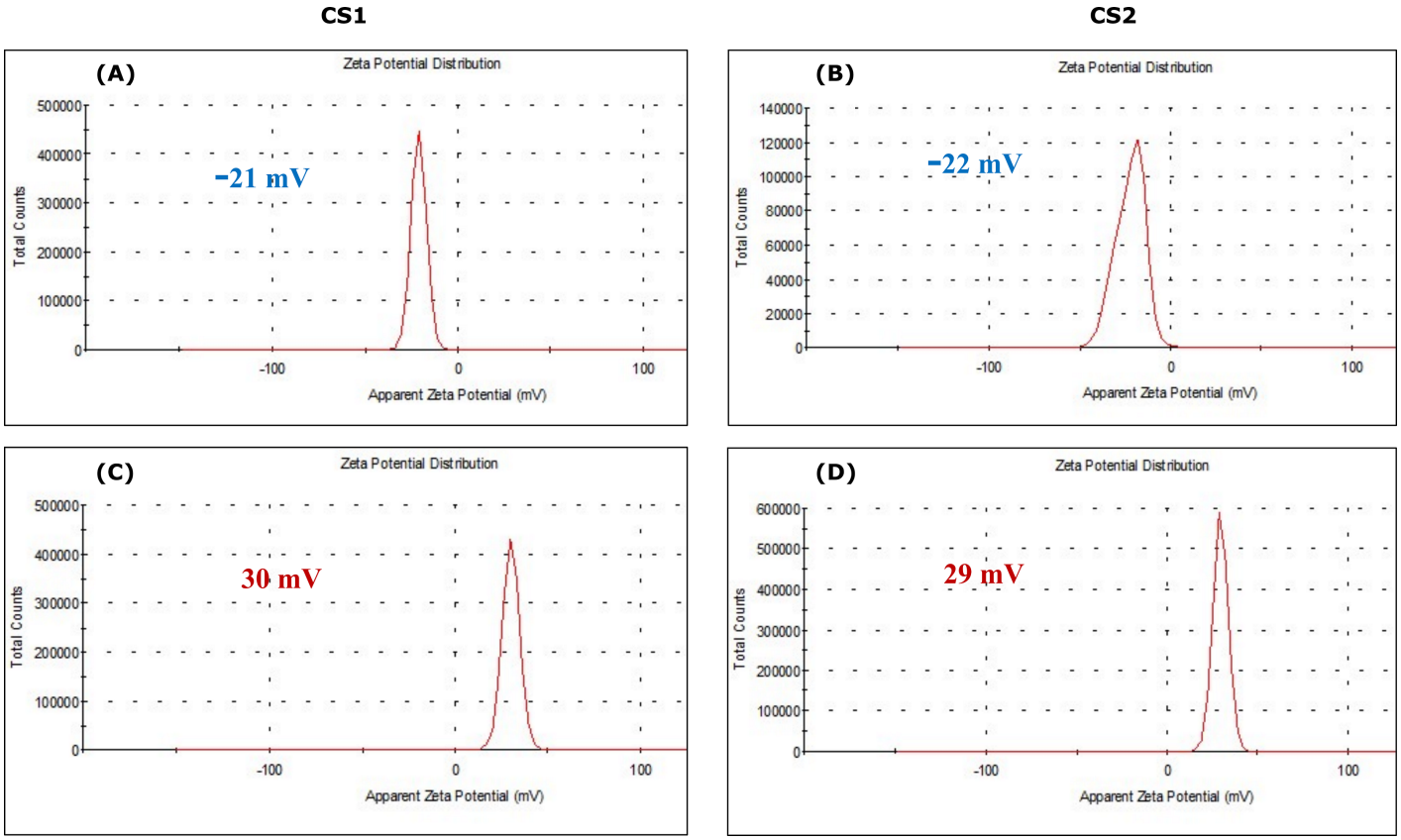

Fig. S1. Zeta potential of PAA-modified core-shell UCNPs CS1 (A) and CS2 (B), showing values of -21 mV and -22 mV, respectively. Upon PEI modification, the zeta potential of UCNPs-PAA CS1 (C) and CS2 (D) shifted to +30 mV and +29 mV, respectively.

S2. Dynamic light scattering DLS of UCNPs-PAA.

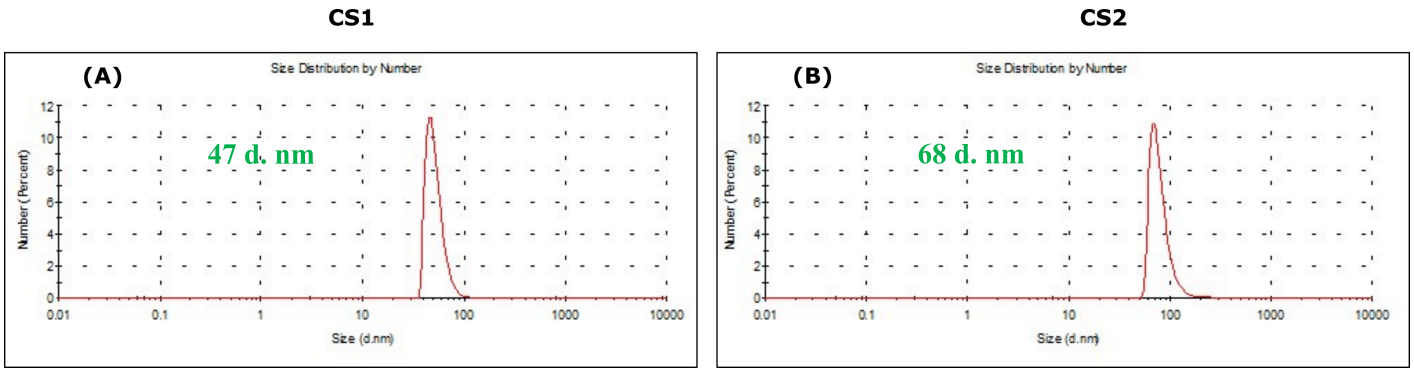

Fig. S2. Dynamic light scattering (DLS) analysis of PAA-modified core-shell UCNPs CS1 (A) and CS2 (B), showing hydrodynamic diameters of 47 nm and 68 nm respectively.

S3. Experimental UCL lifetime measurements system.

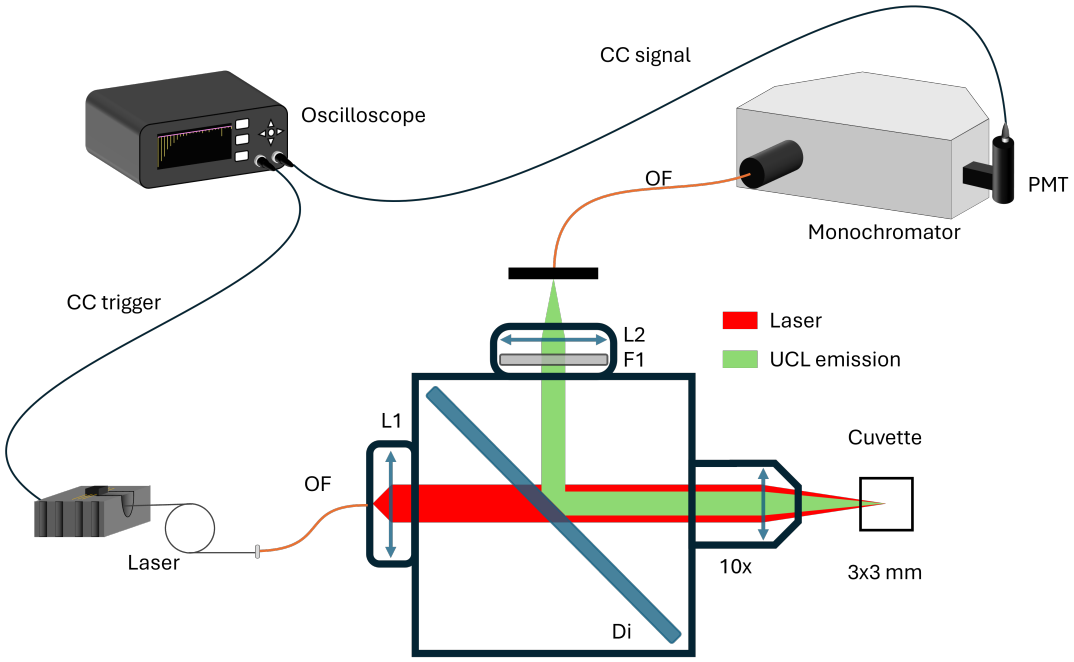

Fig. S3. Schematic of the experimental system to measure the time-resolved UCL. OF: optical fiber; L1: collimating lens; Di: long-pass dichroic filter; 10×: microscope objective; F1: short-pass filter; L2: focusing lens; PMT: photomultiplier tube; CC: coaxial cable.

S4. Fitting procedure for UCL decay curves.

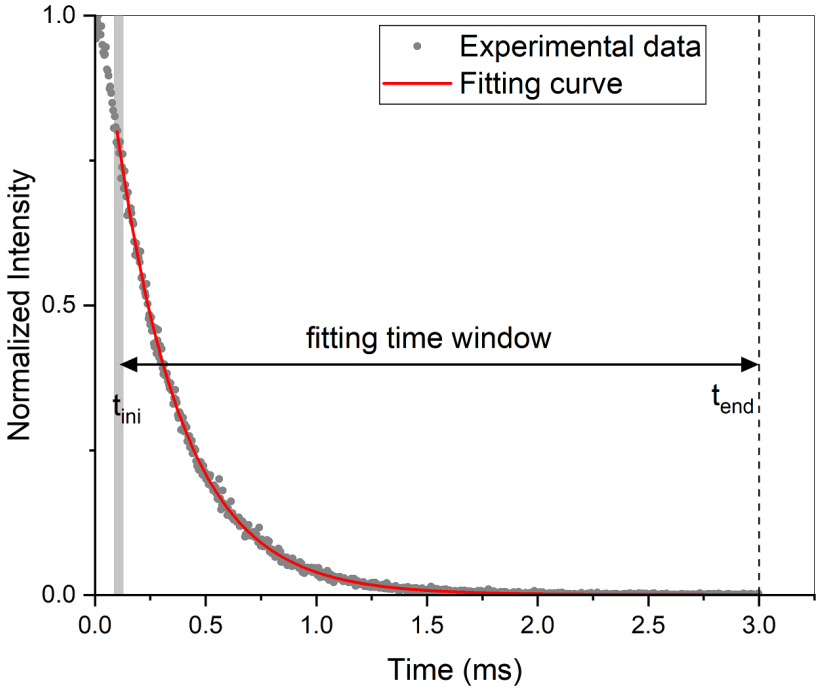

Fig. S4. Fitting procedure of the UCL decay curves. The experimental UCL decay curve (blue line) was fitted to a single-exponential function: $y = y_0 + A\exp(-(t-t_0)/\tau)$, where y_0, A, t_0, and τ are fitting parameters. The fitting was performed over a window from t_{ini} to t_{end} where t_{end} time was set to t_{end} = 3 ms. For each experimental curve, approximately 15 fits were computed by varying the starting time t_{ini} within the region where the luminescence intensity decays from 85% to 75% of its maximum value (indicated by the shaded area). The red line represents one of the individual fitted curves. This fitting procedure yields an average lifetime and its associated standard error. The decay curve shown was recorded under an excitation power of 2.2 W and a pulse width of 10 ms for the sample CS1 without the attached Cy3, resulting in a UCL lifetime of τ= 297 $\pm$ 1 μs.

S5. Measurement of laser beam diameter.

We characterized the laser beam spot size at the sample position by measuring its radius using the knife-edge technique[1]. The UCNP cuvette was positioned to optimize its UCL signal. In the setup used for lifetime measurements, a blade was placed perpendicular to the direction of laser beam propagation, at a position corresponding to the center of the cuvette. A power sensor was placed directly behind the blade to measure the laser beam (Figure S5A). Starting with the beam fully blocked, the power sensor registered values close to zero. As the blade was gradually retracted from the beam path using a translation stage driven by a micrometer screw, the sensor recorded a steadily increasing power. Once the blade was completely out of the beam path, the measured power reached a plateau. At this point, we confirmed that the entire beam was incident on the sensor's active area. Figure S5B shows the recorded power as a function of blade position x, which was fitted to the following expression:

$$P(x) = P_0 + \frac{A}{2}\left[1 + \mathrm{erf}\left(\frac{x - x_C}{w/\sqrt{\ln 2}}\right)\right], \tag{S1}$$

where P_0 is the baseline power, A is the amplitude of the power variation, and the error function (erf) depends on the central position x_C and the beam radius w, which corresponds to the half-width at half-maximum (HWHM), i.e., the distance at which the power reaches half of its maximum value. The fit yielded a beam radius of $w = 120\ \mu$m.

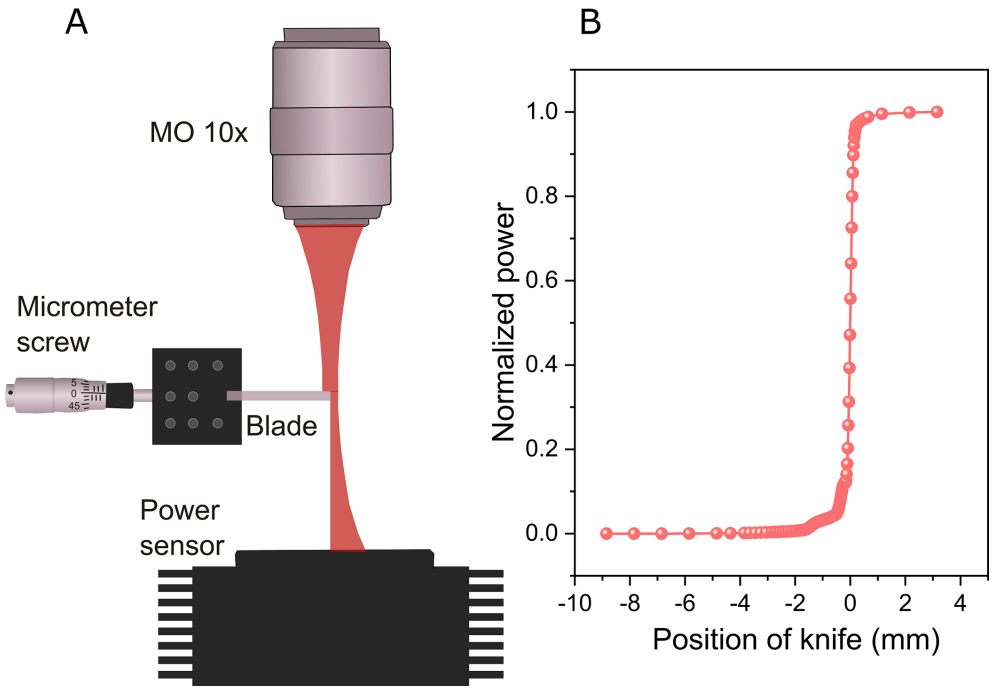

Fig. S5. (A) Schematic of the knife-edge stup: the laser beam exits the microscope objective (MO), is partially blocked by a blade guided by a micrometer screw, and the remaining portion reaches the power sensor. (B) Beam profile at the sample position.

S6. Experimental conditions for the lifetime experiments.

For the experiments involving varying excitation power, the laser pulse width was kept constant at 750 μs. The laser current was adjusted from 1 to 9 A, corresponding to the following equivalent parameters:

Table S 1 Values of laser power and irradiance at the sample position as a function of the laser current. The laser spot diameter used for the irradiance calculation is given in Section S5.

Laser current (A)	**1**	**2**	**3**	**4**	**5**	**6**	**7**	**8**	**9**
Power (W)	**0.3**	**1.0**	**1.6**	**2.2**	**2.9**	**3.6**	**4.2**	**4.9**	**5.5**
Irradiance (W/cm^2)	**729**	**2166**	**3581**	**5018**	**6433**	**7869**	**9306**	**10721**	**12158**

On the other hand, the laser power was kept constant at 2.2 W in the experiment involving variable pulse widths, which are detailed in Table below. For each pulse width, we selected the excitation pulse repetition frequency to ensure complete relaxation of the ions to the ground level before the subsequent excitation pulse, thus avoiding pile-up effects.[2] Accordingly, we employed the minimum repetition frequency allowed by our excitation laser controller (ILX Lightwave, model LDX36025-12) for each pulse width.

Table S 2 Different excitation pulse widths used in the experiments. For each pulse width, the corresponding repetition frequency, period and duty cycle are indicated.

Pulse width (μs)	Repetition frequency (Hz)	Periods (ms)	Duty Cycle (%)
40	125	8	0.5
50	100	10	0.5
60	83.3	12	0.5
70	71.4	14	0.5
100	50	20	0.5
130	38.4	26	0.5
165	30.3	33	0.5
200	25	40	0.5
300	16.6	60.24	0.5
400	12.5	80	0.5
500	10	100	0.5
600	8.3	120.5	0.5
750	6.6	151.5	0.5
1000	5	200	0.5
1000	200	5	20
1500	133.3	7.5	20
2000	100	10	20
3000	66.6	15	20
5000	40	25	20
10000	20	50	20
15000	13.3	75.2	20

S7. Evaluation of the spectral overlap integral.

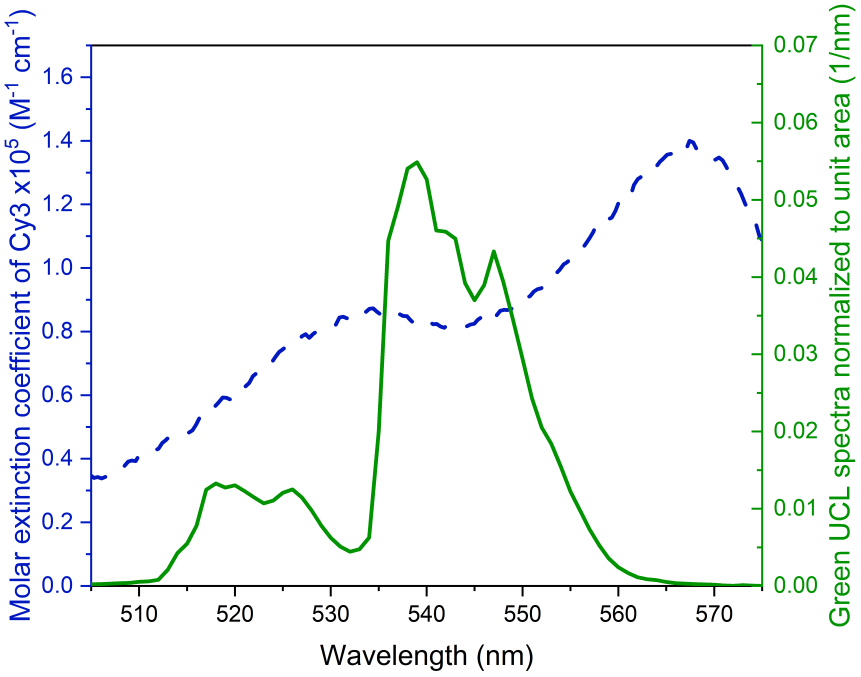

Fig. S6. (Left axis) Molar extinction coefficient spectrum, $\varepsilon_A(\lambda)$, of Cy3. (Right axis) UCL spectrum, $F_D(\lambda)$, normalized to unit area in the green band region (505-575 nm) used to calculate the overlap integral $J = 7 \times 10^{15}$ M^{-1} cm^{-1} nm^4 (see eqn (1)). Note that this value can be roughly estimated by considering a nearly constant value of $\varepsilon_A \simeq 0.8 \times 10^5$ M^{-1} cm^{-1} in the green region of the spectrum around $\lambda = 540$ nm, which gives $J \simeq \varepsilon_A \lambda^4 \simeq 6.8 \times 10^{15}$ M^{-1} cm^{-1} nm^4.

S8. Full temporal evolution of UCL emission.

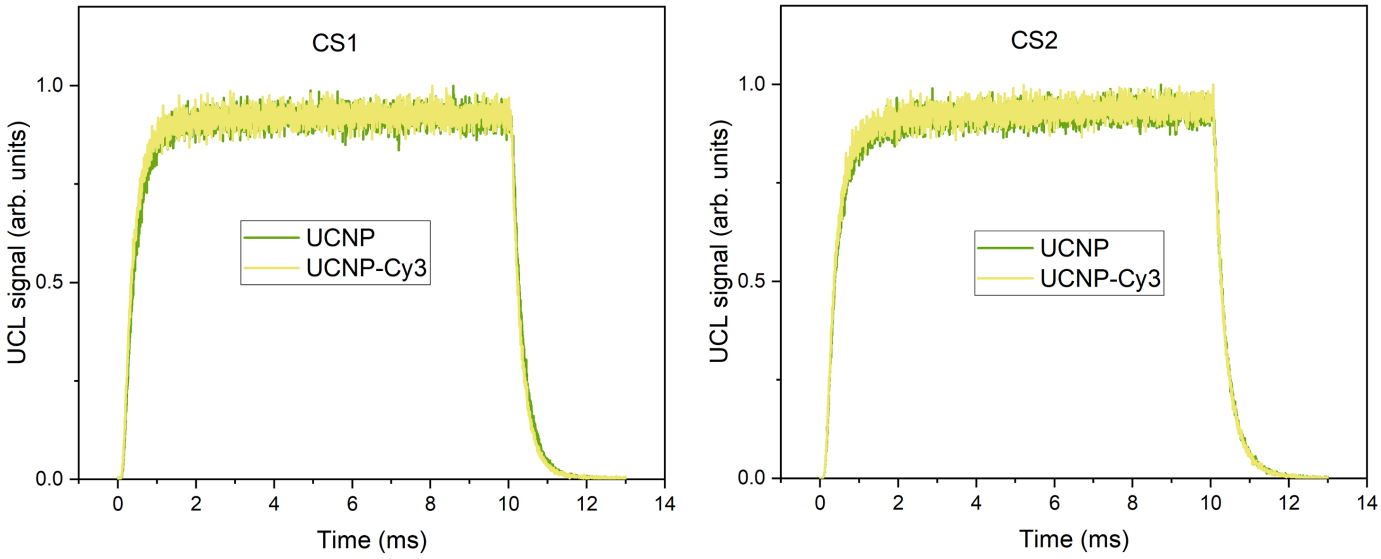

Fig. S7. UCL temporal profile (rise and decay) under 10 ms excitation at 2.2 W, recorded with (yellow line) and without (green line) Cy3. Left: CS1 sample.; Right: CS2 sample.

S9. Temporal profile of Cy3 emission.

We analyzed the temporal evolution of Cy3 emission (around 580 nm). The excited-state population of Cy3 is governed primarily by two processes: (1) energy transfer from the green-emitting Er^{+3} level, which acts as the excitation source, and (2) rapid de-excitation of the Cy3 molecules. Since the intrinsic relaxation time of Cy3 is much shorter than the characteristic decay times of Er^{+3} levels, it is reasonable to assume that the Cy3 excited-state population adiabatically follows the dynamics of the Er^{+3} donor level. Consequently, the temporal profile and decay kinetics of the Cy3 emission should largely mirror those of the green UCL signal. To test this experimentally, we measured the decay curves at 582 nm for various excitation pulse widths. These curves revealed an additional faster decay component not present in the green emission. As an example, in Figure S8A, we compare the decay curves measured at 540 nm (corresponding to the Er^{+3} green emission) and at 582 nm (corresponding to the Cy3 emission) for an excitation pulse width of 200 μs. The decay curve at 582 nm clearly exhibits a fast initial drop, followed by a slower decay that matches the one observed at 540 nm. To further investigate this behavior, we fitted the decay curves at 582 nm using a biexponential model. Across all pulse widths, we consistently observed two components: a fast decay in the range of tens of microseconds, and a slower decay matching the Er^{+3} emission at 540 nm. These results are shown in Figure S8B: solid symbols represent the UCL lifetimes obtained at 540 nm (with and without Cy3) (Figure 2C of the manuscript), while open symbols correspond to the slower decay component extracted from the 582 nm signal. This confirms that the Cy3 emission corresponds to the Er^{+3} donor dynamics, as expected. However, the presence of the faster decay component suggests an additional process such as a spectral or dynamic overlap between Cy3 emission and secondary Er^{3+} transitions.

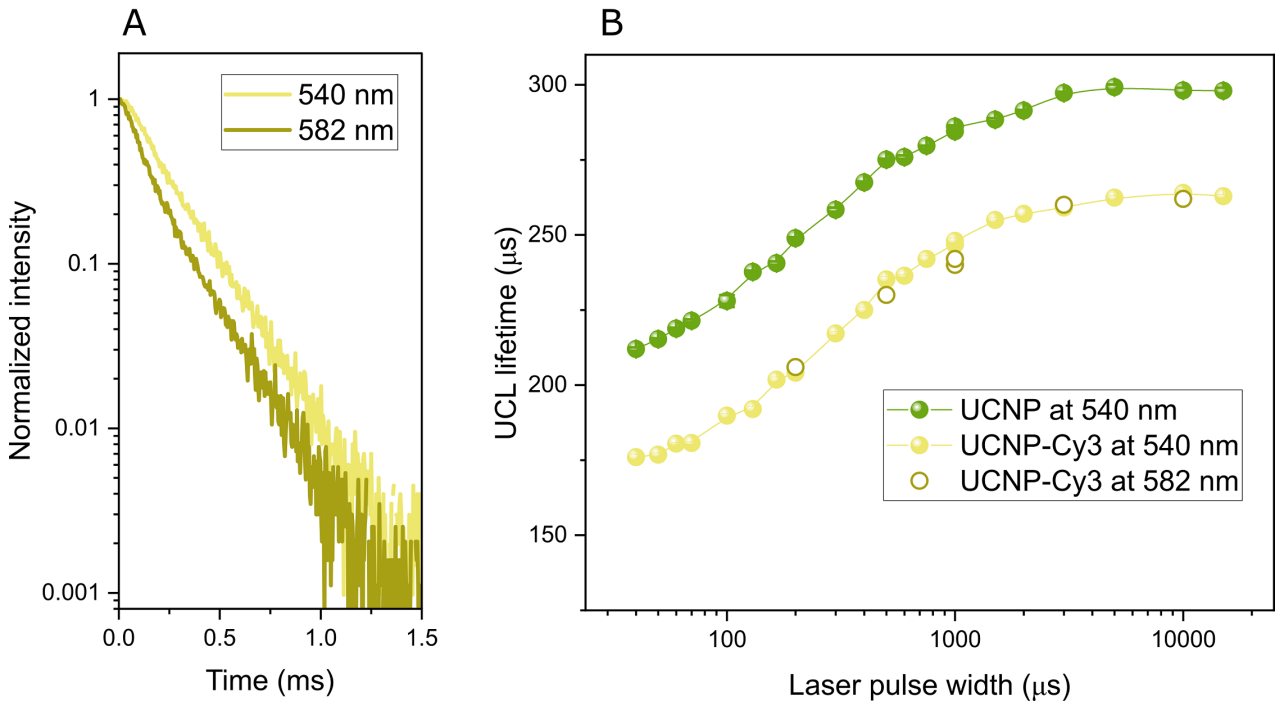

Fig. S8. (A) Decay curves of the CS1 sample measured at 540 nm and 582 nm under a 200 μs excitation pulse. (B) UCL lifetimes extracted from decay curves at 540 nm with and without Cy3 (from Figure 2C of the manuscript) and the slower decay component measured at 582 nm, which matches the one measured at 540 nm.

S10. Parameter values used in the theoretical model.

The parameter values used in the theoretical model closely match those reported in the literature.[3–7] Additionally, some of these parameters were adjusted as control variables to accurately reproduce the experimental results. The decay time of the Yb^{3+} ions in level 1 is approximately two milliseconds, for which we used $1/W_{Yb1} = 1.9$ ms. The absorption cross-section of the Yb^{3+} transition at the laser wavelength is $\sigma_{Yb1} = 2.3 \times 10^{-21}$ cm^2, leading to a calculated saturation intensity of $I_{sat} = 2.4 \times 10^4$ W/cm^2. To estimate the concentration of Er^{3+} (N_{Er}) and Yb^{3+} (N_{Yb}) ions, we followed the molecular weight calculation method for UCNPs proposed by Mackenzie et al.[8] Using the hexagonal crystal lattice parameters $a_h = 0.596$ nm and $c_h = 0.353$ nm. we determined the unit cell volume as $u_V \simeq 0.1086$ nm^3. By considering the fractional percentage of rare-earth (RE) dopants f_{RE} ($RE = Yb$ and Er), the RE ion concentration was computed as $N_{RE} = 1.5 f_{RE}/u_V$, resulting in $N_{Yb} = 2.8 \times 10^{21}$ cm^{-3} and $N_{Er} = 2.8 \times 10^{20}$ cm^{-3}. The decay times of Er^{3+} ion energy levels range from the milliseconds, particularly for transitions to the ground state, to microseconds when non-radiative contributions are considered. The longest decay time corresponds to the metastable level 1 ($^4I_{13/2}$), which radiatively decays to the ground state ($^4I_{15/2}$) on a millisecond scale, we adopted $1/W_{Er1} = 5$ ms. Determining the exat values of all decay times, as well as resonant energy transfer and cross-relaxation coefficients, is challenging. Since we use a homogeneous rate equation model, these parameters represent global values for the entire ion ensemble. Therefore, starting with values from the liteture[3–7], we performed an optimization process to fit our experimental data. This optimization was carried out using the *fminsearch* function in Matlab. The radiative decay rates of excited levels to the ground state remain in the millisecond range, where we set $1/W_{Er20} = 1.2$ ms and $1/W_{Er30} = 1/W_{Er40} = 0.5$ ms. Faster non-radiative decay processes occur on the microsecond scale, for which we used $W_{Er21} = 8.5 \times 10^3$ s^{-1}, $W_{Er32} = 8.5 \times 10^3$ s^{-1}, and $W_{Er43} = 5 \times 10^3$ s^{-1}. Regarding energy transfer from Yb^{3+} to Er^{3+} ions, we set the parameters as follows: $K_2 = 0.8 \times 10^{-16}$ cm^3 s^{-1}, $K_4 = 0.2 \times 10^{-16}$ cm^3 s^{-1}, with lower values for $K_3 = 0.02 \times 10^{-16}$ cm^3 s^{-1} and for the back energy transfer $K_{B2} = 0.08 \times 10^{-16}$ cm^3 s^{-1}. The energy transfer coefficients between neighbors Er^{3+} ions were set to $C_{Er1} = 1 \times 10^{-17}$ cm^3 s^{-1} and $C_{Er2} = 1.9 \times 10^{-17}$ cm^3 s^{-1}.

Finally, we estimated the FRET rate $W_{Er4FRET}$, which quantifies the strength of the interaction between the UCNP and Cy3 molecules. Using the FRET efficiency definition (Equation (6)), the rate was calculated as follows:

$$W_{Er4FRET} = \frac{(W_{Er40} + W_{Er43})\, E_{FRET}}{(1 - E_{FRET})} \,. \tag{1}$$

By applying a FRET efficiency of $E_{FRET} = 29\%$, as obtained from steady-state measurements of the CS1 UCNPs, we determined a value of $W_{Er4FRET} = 2859$ s^{-1}.

Table S 3 Description of representative physical parameters for the Yb^{3+}-Er^{3+} system reported in the literature, along with the specific values used in the simulations performed in this work.

Physical parameter	Reported values (ref.)	Value used in this work
W_{Yb1} (s^{-1})	645–613 [3] 6225 [6] 1000 [7]	531
W_{Er1} (s^{-1})	110 [3] 100 [4] 350 [6] 250 [7]	198
W_{Er20} (s^{-1})	73–130 [3] 128 [4] 73 [6] 1250 [7]	802
W_{Er30} (s^{-1})	2039–2770 [3] 870 [4] 2950 [6] 2500 [7]	2180
W_{Er40} (s^{-1})	880–1510 [3] 1220 [4] 1510 [6] 2500 [7]	2000
W_{Er21} (s^{-1})	32–61 [3] 81 [4] 1000 [6] 10000 [7]	8500
W_{Er32} (s^{-1})	9000 [4] 10000 [7]	8500
W_{Er43} (s^{-1})	26–1892 [3] 765 [4] 820 [6] 10000 [7]	5000
K_2 (cm^3 s^{-1})	5.2×10^{-18} [6] 7.5×10^{-17} [7]	0.8×10^{-16}
K_{2B} (cm^3 s^{-1})	K_2/K_{2B}=6–8 [3] 3.5×10^{-16} [6] 1.5×10^{-17} [7]	0.08×10^{-16}
K_3 (cm^3 s^{-1})	0 [3] 0 [7]	0.02×10^{-16}
K_4 (cm^3 s^{-1})	$1.54–2.64 \times 10^{-15}$ [3] 8.7×10^{-14} [6] 7.5×10^{-17} [7]	0.2×10^{-16}
C_{Er1} (cm^3 s^{-1})	$1.9–2.31 \times 10^{-17}$ [3] 3×10^{-17} [4] 2.3×10^{-17} [6] 0.9×10^{-17} [7]	1×10^{-17}
C_{Er2} (cm^3 s^{-1})	1.8×10^{-17} [4] 1.8×10^{-17} [7]	1.9×10^{-17}

References

1 M. A. de Araújo, R. Silva, E. de Lima, D. P. Pereira and P. C. de Oliveira, *Appl. Opt.*, 2009, **48**, 393–396.

2 L. Labrador-Páez, U. Kostiv, Q. Liu, Y. Li, H. Ågren, J. Widengren and H. Liu, *The Journal of Physical Chemistry Letters*, 2022, **13**, 11208–11215.

3 R. B. Anderson, S. J. Smith, P. S. May and M. T. Berry, *The Journal of Physical Chemistry Letters*, 2014, **5**, 36–42.

4 N. U. Wetter, A. M. Deana, I. M. Ranieri, L. Gomes and S. L. Baldochi, *IEEE Journal of Quantum Electronics*, 2010, **46**, 99–104.

5 S. Fischer, H. Steinkemper, P. Löper, M. Hermle and J. C. Goldschmidt, *Journal of Applied Physics*, 2012, **111**, 013109.

6 M. Kaiser, C. Würth, M. Kraft, T. Soukka and U. Resch-Genger, *Nano Research*, 2019, **12**, 1871–1879.

7 A. Casillas-Rubio, D. Mendez-Gonzalez, M. Laurenti, J. Rubio-Retama, O. G. Calderón and S. Melle, *Nanoscale*, 2024, **16**, 12184–12195.

8 L. E. Mackenzie, J. A. Goode, A. Vakurov, P. P. Nampi, S. Saha, G. Jose and P. A. Millner, *Sci Rep*, 2018, **8**, 1106.